

Gamma-ray polarization induced by cold electrons via Compton processes

Zhe Chang^{1,2,*}, Yunguo Jiang^{1,2,†}, Hai-Nan Lin^{1,‡}

¹*Institute of High Energy Physics
Chinese Academy of Sciences, 100049 Beijing, China*

²*Theoretical Physics Center for Science Facilities
Chinese Academy of Sciences, 100049 Beijing, China*

Abstract

The polarization measurement is an important tool to probe the prompt emission mechanism in gamma-ray bursts (GRBs). The synchrotron photons can be scattered by cold electrons in the outflow via Compton scattering processes. The observed polarization depends on both the photon energy and the viewing angle. With the typical bulk Lorentz factor $\Gamma \sim 200$, photons with energy $E > 10$ MeV tend to have smaller polarization than photons with energy $E < 1$ MeV. At the right viewing angle, i.e. $\theta \sim \Gamma^{-1}$, the polarization achieves its maximal value, and the polarization angle changes 90° relative to the initial polarization direction. Thus, the synchrotron radiation plus Compton scattering model can naturally explain the 90° change of the polarization angle in GRB 100826A.

Subject headings: Gamma-ray burst: general - Polarization - Scattering

1. Introduction

Although a remarkable advance of investigations on GRBs was made in the past decades, the mechanism of the prompt emission of GRBs is still unclear. The optically thin synchrotron radiation (SR) is believed to be the most promising mechanism to produce a broken power law spectrum, i.e. the empirical Band function (Band et al. 1993). One supporting evidence is from the ‘‘Amati relation’’, which states that the peak energy of the νF_ν spectrum E_{peak} is correlated with the isotropic equivalent radiation energy E_{iso} (Amati et al 2002; Amati 2006). However, there are still some disputes in the low energy regime, namely the prediction of the SR in the fast cooling phase $\alpha \sim -3/2$ is against a large number of the observed samples $\alpha \sim -1$ (Preece et al. 2000).

* changz@ihep.ac.cn

† jiangyg@ihep.ac.cn

‡ linhn@ihep.ac.cn

Essentially, the inverse Compton (IC) process combined with the SR will change the distribution of the electrons and influence the spectra. Daigne et al. (2011) also indicated that α in the marginally fast cooling case can be up to $-2/3$, and the majority of the observed GRB prompt phase can be reconciled with the synchrotron origin. The SR process produces polarized light beams, the polarimetric observation of the prompt emission will provide us more information beyond the spectrum and the light curve. The time lags between GeV and MeV photons in GRBs were used to constraint the Lorentz invariance violation (LIV) effects (Chang et al. 2012a), and the polarization observation can be used to constraint the CPT violation effects (Toma et al. 2012). Many issues of polarizations in GRBs were investigated both theoretically and experimentally.

Theoretically, the gamma-ray polarization depends on both the emission mechanism and the geometry of the outflow. For synchrotron origin in the prompt phase, the maximal polarization is $\Pi_{\max} = (p + 1)/(p + 7/3)$, if the spectrum of electrons has a power-law index p and the magnetic field is uniform at large scale in the plasma (Rybicki & Lightman 1979). The configuration of the magnetic field is essential to produce the polarization. Granot (2003) indicated that an ordered magnetic field can produce $\Pi \geq 50\%$ easily, and the magnetic field component orthogonal to the moving direction of the outflow produce smaller Π than the one parallel to the moving direction. Lyutikov et al. (2003) calculated the stokes parameters and derived the pulse-averaged polarization with a given toroidal magnetic field. They showed that $\Pi \sim 56\%$ can be achieved for viewing angles larger than $1/\Gamma$ and the observed maximum polarization is smaller than that due to the relativistic kinematic effect. Nakar et al. (2003) showed that the SR from random magnetic fields can lead to $\Pi \sim 30 - 35\%$, while a uniform field produces $\Pi \sim 45 - 50\%$. However, a significant polarization can be obtained if the line of sight is within the small jet open angle $\theta_{\text{jet}} \sim \Gamma^{-1}$.

The synchrotron origin is widely accepted as the successful theory to explain the GRB afterglows (Sari et al. 1998). The polarization in the afterglow phase has also been studied by several works (Gruzinov & Waxman 1999; Gruzinov 1999; Sari 1999). Gruzinov & Waxman (1999) showed $\Pi \cong \Pi_{\max}/\sqrt{N}$, where N is the number of the magnetic field patches in the visible region. Sari (1999) investigated the polarization on the averaged emission site in the afterglow, and showed that the observed Π is not likely to exceed 20%. Considering the dynamics of the jet, the polarization direction will change 90° before and after the jet breaking time for an observer moving away from the jet center. Although observations of the optical afterglow of GRB 021004 and GRB 020405 showed a possible polarization evolution in both the direction and the degree, the cosmic dust contribution ($\sim 1\%$) can not be unambiguously excluded (Lazzati et al. 2003; Covino et al. 2003). A recently observed GRB 091018 confirmed the polarization evolution theory (Wiersema et al. 2012). Rossi et al. (2004) studied the jet structure effects on the polarization in the afterglow.

As stated above, the IC processes are essential to understand the prompt emission mechanism. The IC induced polarizations were also studied by several authors (Shaviv & Dar 1995; Lazzati et al. 2004; Eichler & Levinson 2003; Levinson & Eichler 2004; Toma et al. 2009). Shaviv & Dar (1995) showed that the IC scattering can explain many features of the GRBs, such as the temporal features, multi-peak light curves, power-law spectra in the high energy regime, and also the polar-

ization prediction. Lazzati et al. (2004) discussed the IC induced polarization in the point source limit, and indicated that Π can be large after the proper angular integration when a certain special geometry of the jet is realized. Toma et al. (2009) used the Monte Carlo methods to distinguish GRB polarizations produced in three different scenarios: the SR with a global ordered magnetic field (SO) model, the SR with random magnetic fields model and the Compton drag model. The simulation showed that the Compton drag model is favored when $\Pi > 0.8$, and the SR with ordered magnetic fields model is favored when $\Pi \sim 0.2 - 0.7$.

The early age observations of the polarization concerned mainly the optical and radio bands, and the typical value of Π is less than 10% for many GRBs in the afterglow phase (Taylor et al. 1998; Frail et al. 1998; Hjorth et al. 1999; Wijers et al. 1999; Bersier et al. 2003; Greiner et al. 2003; Steele et al. 2009). The first large linear polarization in the prompt emission was reported by *RHESSI* from GRB 021206 (Coburn & Boggs 2003), although this result was challenged by other independent groups (Rutledge & Fox 2004; Wigger et al. 2004). The recent detection of the polarization in the prompt phase indicated very large polarizations in GRB 041219A, GRB 100826A, GRB 110310 and GRB 110721A (McGlynn et al. 2007; Kalemci et al. 2007; Götz et al. 2009; Yonetoku et al. 2011, 2012; Toma et al. 2012). We give a summary of these results in Table 1. From the data, one can see that it is possible that the polarization in the prompt phase is larger than 80%, which is beyond the maximal value of the SR induced polarization. Thus, the SR plus Compton scattering (CS) model is worth investigating. We wish that the initial polarization of SR photons and CS effect can not only supply a reasonable framework for observed GRB polarization, but also presents a consistent scenario for the spectra, the light curves, and the polarizations.

The present paper is organized as follows. In Section 2, we introduce the SR plus CS model, derive the polarization formula in the observer frame, and show the characteristics of the model. In Section 3, we use this SR and CS effect combined model to discuss four GRB cases. The conclusion and remarks are given in Section 4.

2. Polarization induced by cold electrons via Compton scattering

In the standard fireball model, a jet expands outwards from the central engine, and finally coasts with a large bulk Lorentz factor Γ . In the most forward layer of the jet, the internal energy can be ignored, and the electrons are considered to be non-relativistic in the comoving frame. In the inner part of the jet, the internal shock accelerates electrons, leading to the SR in the presence of magnetic fields. Therefore, the synchrotron photons will illuminate the cold electron layer and be scattered by electrons via Compton processes. This process is different from the upper scattering Compton process, since the latter transfers the energy from electrons to photons, while the former transfers energy inversely. The optical depth is given as $\tau \equiv n\sigma_T r/\Gamma = L\sigma_T/4\pi r m_p c^3 \Gamma^3$, where L is the isotropic luminosity, σ_T is the Thomson cross section (Chang et al. 2012a). For the typical Gamma-ray burst parameters, $L \sim 10^{52}$ erg \cdot s $^{-1}$ and $\Gamma \sim 10^3$, τ is less than 1 in the region of $r > 10^{10}$ cm. Thus, one reasonable assumption is that one photon is scattered at most once by the

Table 1. Polarizations in observation

GRB	Redshift	Energy Band	Polarization	Phase	References
GRB 980329	~ 3.5	radio	$< 21 \%$ (2σ)	afterglow	[1]
GRB 990123	1.61	optical	$< 2.3 \%$	afterglow	[2]
GRB 990510	1.619	optical	$< 1.7 \%$	afterglow	[3], [4]
GRB 020405	0.695	optical	$< 10 \%$	afterglow	[5]
GRB 021206	/	γ -ray	$< 100 \%$	prompt	[6],[7]
GRB 030329	0.168	optical	$0.3 \sim 2.5 \%$	afterglow	[8], [9]
GRB 041219A	~ 0.3	γ -ray	$98 \pm 33 \%$	prompt	[10], [11]
GRB 090102	1.547	optical	$10 \pm 1 \%$	afterglow	[12]
GRB 091208B	1.063	optical	$10.4 \pm 2.5 \%$	afterglow	[13]
GRB 100826A	/	γ -ray	$27 \pm 11 \%$ (2.9σ)	prompt	[14]
GRB 110301A	/	γ -ray	$70 \pm 22 \%$ (3.7σ)	prompt	[15]
GRB 110721A	0.382 ^a	γ -ray	$88_{-28}^{+16} \%$ (3.3σ)	prompt	[15], [16]

^aThere is a caution that the afterglow observations of GRB 110721A were inconclusive, another candidate redshift is 3.512 (Berger et al. 2011).

References. — [1] Taylor et al. (1998); [2] Hjorth et al. (1999); [3] Covino et al. (1999); [4] Wijers et al. (1999); [5] Bersier et al. (2003); [6] Rutledge & Fox (2004); [7] Wigger et al. (2004); [8] Greiner et al. (2003); [9] Caldwell et al. (2003); [10] McGlynn et al. (2007); [11] Kalemci et al. (2007); [12] Steele et al. (2009); [13] Uehara et al. (2012); [14] Yonetoku et al. (2011); [15] Yonetoku et al. (2012) [16] Berger et al. (2011).

electrons in the forward layer of the jet.

The set-up of this system is given in Figure 1. The SR photons are collimated along the moving direction of the outflow, namely the \hat{z} -direction, scattered off by a static electron at the \mathcal{O} point, and then travel towards the observer in the \hat{n} -direction. The angle between \hat{z} and \hat{n} is θ . The initial polarization is defined as $\Pi_0 = (I'_{\parallel} - I'_{\perp})/(I'_{\parallel} + I'_{\perp})$, where the intensities I'_{\parallel} and I'_{\perp} correspond to the electric components E_0^{\parallel} and E_0^{\perp} (see Figure 1), respectively. We use the convention that the variable with a prime is in the comoving frame. Consider an incident photon with energy ε'_0 , the photon energy after scattering in the comoving frame is given by

$$\varepsilon'_1 = \frac{\varepsilon'_0}{1 + \frac{\varepsilon'_0}{m_e c^2} (1 - \cos\theta')}. \quad (1)$$

The cross section (the Klein-Nishina formula) reads

$$d\sigma = \frac{r_0^2}{4} d\Omega' \left(\frac{\varepsilon'_1}{\varepsilon'_0} \right)^2 \left[\frac{\varepsilon'_1}{\varepsilon'_0} + \frac{\varepsilon'_0}{\varepsilon'_1} - 2 + 4\cos^2\Theta' \right], \quad (2)$$

where $r_0 \equiv e^2/m_e c^2$ is the classical electron radius, and Θ' is the angle between the polarization direction before and after the scattering. The polarization is defined to be

$$\Pi' \equiv \frac{J'_{\parallel} - J'_{\perp}}{J'_{\parallel} + J'_{\perp}}, \quad (3)$$

where the intensities J'_{\parallel} and J'_{\perp} are written as

$$J'_{\parallel} d\Omega' = I'_{\parallel} d\sigma (\Theta' = \theta') + I'_{\perp} d\sigma (\Theta' = \pi/2), \quad (4)$$

$$J'_{\perp} d\Omega' = I'_{\parallel} d\sigma (\Theta' = \pi/2) + I'_{\perp} d\sigma (\Theta' = 0), \quad (5)$$

respectively. Substituting Equations (2), (4) and (5) into Equation (3), one obtains the polarization in the comoving frame

$$\Pi'(\theta') = \frac{\Pi_0(1 + \cos^2\theta') - \sin^2\theta'}{\varepsilon'_1/\varepsilon'_0 + \varepsilon'_0/\varepsilon'_1 - (1 + \Pi_0)\sin^2\theta'}. \quad (6)$$

Since the incident photons are of the synchrotron origin, the initial polarization is $\Pi_0 = (p+1)/(p+7/3)$, where p is the power-law index of the electron distribution ($N(\gamma') \propto \gamma'^{-p}$) (Rybicki & Lightman 1979). The polarization is invariant under Lorentz transformation (Cocke & Holm 1972). One has $\Pi'(\theta') = \Pi(\theta)$, where θ is the angle in the observer frame. The Lorentz transformation of the angle θ' to the observer frame is expressed as

$$\cos\theta' = \frac{\cos\theta - \beta}{1 - \beta\cos\theta}, \quad (7)$$

where $\beta \equiv \sqrt{1 - 1/\Gamma^2}$ is the velocity of the jet in unit of the light speed. The inverse transformation gives $\cos\theta = (\cos\theta' + \beta)/(1 + \beta\cos\theta')$, therefore $\theta \ll 1$ for $\beta \approx 1$. The Doppler effect leads to

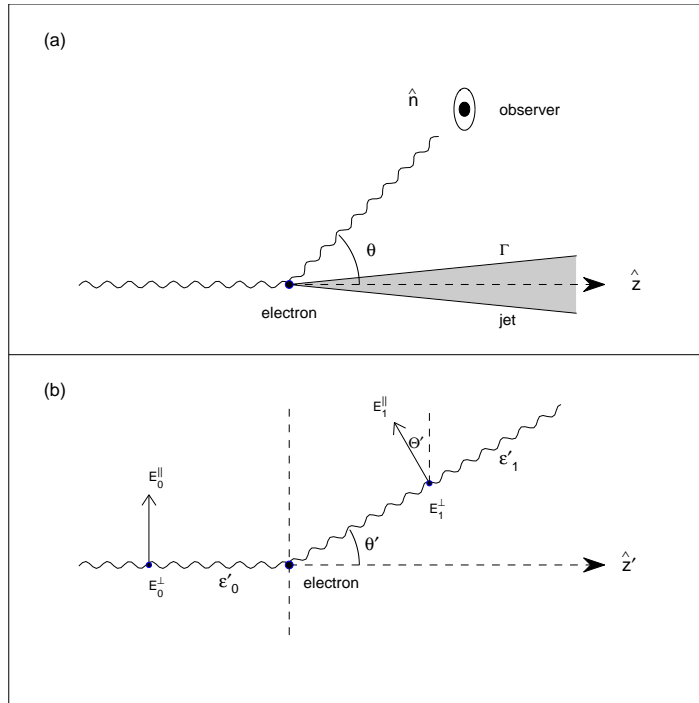


Fig. 1.— Schematic description of the CS processes. The top panel depicts an incident photon scattered in the observer frame. The bottom panel describes the decomposition of electric vector before (E_0) and after (E_1) the scattering process in the comoving frame. The parallel direction (\parallel) and transverse direction (\perp) are defined to be in and orthogonal to the scattering plane, respectively.

$\varepsilon'_0 = \mathcal{D}_0^{-1}\varepsilon_0$ and $\varepsilon'_1 = \mathcal{D}^{-1}\varepsilon_1$, where $\mathcal{D}_0 = 1/\Gamma(1 - \beta)$ and $\mathcal{D} = 1/\Gamma(1 - \beta \cos \theta)$ are the Doppler factors. One has such relation

$$\Sigma \equiv \frac{\varepsilon'_1}{\varepsilon'_0} = 1 - \frac{\Gamma\varepsilon_1}{m_e c^2}(1 - \cos \theta)(1 + \beta). \quad (8)$$

Since Σ is positive, we should require $\varepsilon_1 < m_e c^2/[\Gamma(1 - \cos \theta)(1 + \beta)] \approx m_e c^2/\Gamma\theta^2$. When θ goes to zero, this limit is not complete. The spectrum of the incident photons can be described by the Band function in most GRBs, we use ε_{\max} to denote the upper limit of the high energy band. Since the incident photons lose energy to the static electrons in the scattering processes, another limit is $\varepsilon_1 < \varepsilon_{\max}$. Therefore, ε_1 must satisfy

$$\varepsilon_1 < \min\{\varepsilon_{\max}, m_e c^2/\Gamma\theta^2\}. \quad (9)$$

Based on Equations (7) and (8), the polarization in the observer frame is written as

$$\Pi(\varepsilon_1, \theta) = \frac{\Pi_0[(1 + \cos^2\theta)(1 + \beta^2) - 4\beta\cos\theta] - (1 - \beta^2)\sin^2\theta}{(1 - \beta\cos\theta)^2(\Sigma + \Sigma^{-1}) - (1 - \beta^2)(1 + \Pi_0)\sin^2\theta}, \quad (10)$$

where Σ is given in Equation (8). Therefore, the observed polarization is a function of both the observation angle θ and the observed photon energy ε_1 .

In Figure 2, we present the plots of the observed polarization at different viewing angles in the observer frame. The shape of the curves depends on the bulk Lorentz factor of the GRB outflow. For a typical long GRB, Chang et al. (2012b) showed that the bulk Lorentz factor is approximately 200. Thus, we set $\Gamma = 200$ in the numerical calculation. The initial polarization is set to be $\Pi_0 = 0.75$ for the top panel, which is a typical value of the SR induced polarization. For small viewing angle, i.e. $\Gamma\theta \ll 1$, Π is roughly the same with Π_0 for photons with different energies. When $\Gamma\theta \sim 1$, the polarization direction changes 90° and the polarization approaches 100% for small energy photons, i.e., $\varepsilon_1 \leq 1$ MeV. As the energy increases, the polarization starts to decrease at this special viewing angle. For instance, $\Pi < 20\%$ for $\varepsilon_1 > 100$ MeV. For $\varepsilon_1 = 0.01$ MeV, Π goes back to the initial Π_0 in large viewing angles, and also the polarization direction returns. However, for the $\varepsilon_1 = 1$ MeV, Π decreases to zero at $\Gamma\theta \sim 10$. The regime in the parameter space of $\varepsilon_1 = 1$ MeV and $\Gamma\theta > 10$ is excluded by the constraint in Equation (9), we cut off the curves for high energy photons. When the energy of photons is 10 MeV, the polarization will be less than 40% at the second peak. Even at $\Gamma\theta \sim 1$, the polarization starts to decrease for $\varepsilon_1 = 25$ MeV. The curve of 100 MeV shows that the polarization almost shrinks to 0 for $\Gamma\theta = 1$.

If the initial light beam is unpolarized, i.e. $\Pi_0 = 0$, the CS process can still cause polarization (Shaviv & Dar 1995; Lazzati et al. 2004; Toma et al. 2009). In the bottom panel of Figure 2, the polarization as a function of different viewing angles for different energies is plotted. For photons with energy less than 1 MeV, Π gets the maximal value 100% at $\Gamma\theta = 1$, and approaches to zero quickly when $\Gamma\theta > 5$. This is the result of the Compton induced polarization in the Thomson limit. Thus, one can observe completely polarized gamma-rays at viewing angle $\theta \sim \Gamma^{-1}$ in the prompt

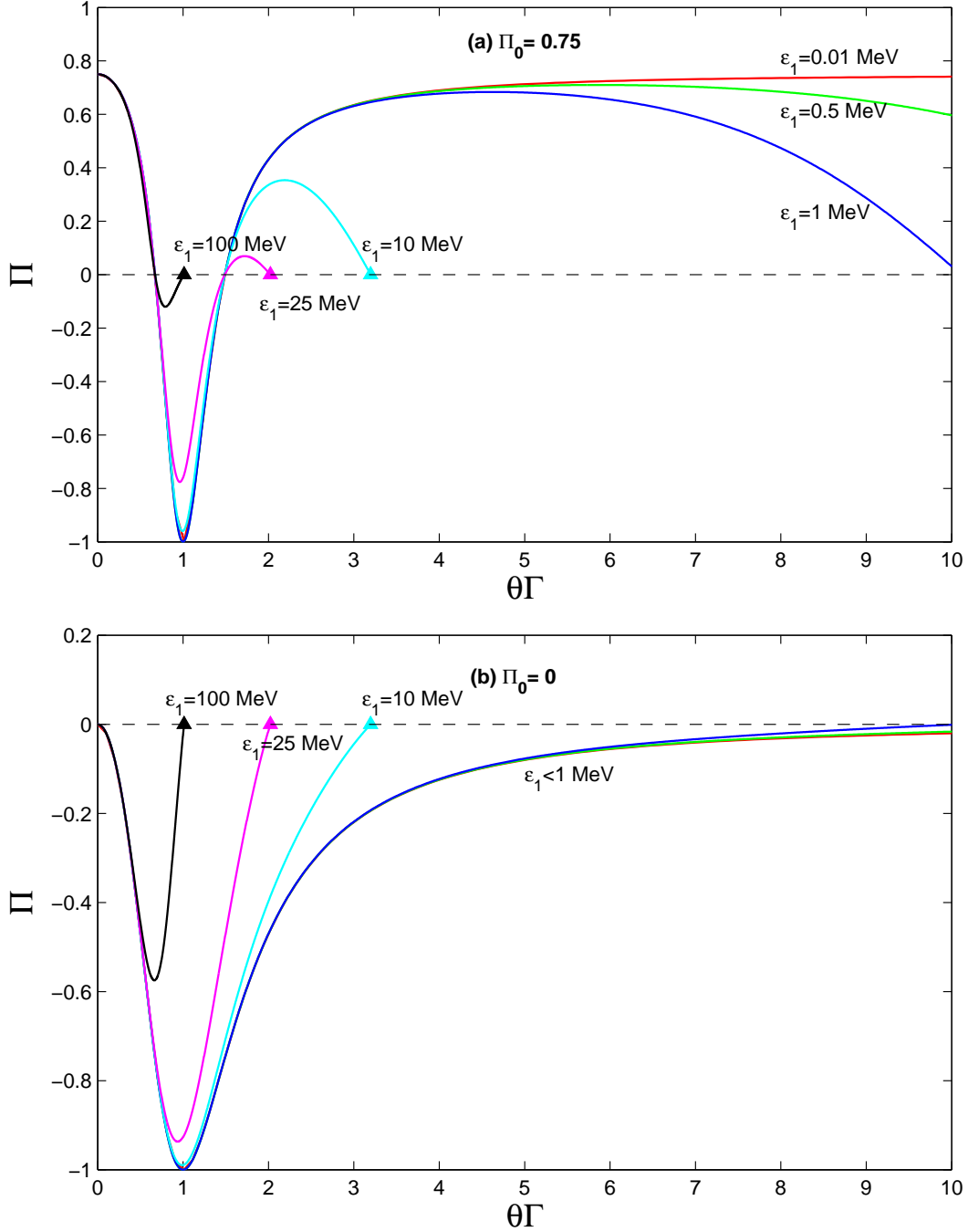


Fig. 2.— Polarization as a function of the observing angle. The initial polarization is set to be $\Pi_0 = 0.75$ in the top panel, and $\Pi_0 = 0$ in the bottom panel. Polarization curves for photons with various energies $\varepsilon_1 = 0.01, 0.5, 1, 10, 25$ and 100 MeV are plotted.

phase. However, the polarization of 10 MeV photons decrease to zero at $\Gamma\theta \sim 3$. The reason is that the Klein-Nishina effects start to influence the polarization for high energy photons. For $\varepsilon_1 = 100$ MeV, Π decreases to 60% at the first “valley”, but goes to 0 at $\Gamma\theta \sim 1$. The similar curves emerge in both panels, which can be attributed to the Klein-Nishina effects. In both $\Pi_0 = 0$ and $\Pi_0 = 0.75$ cases, the polarization of high energy photons is smaller than that of low energy photons. This characteristic is different from the polarization caused by the SR, and can be used to distinguish the polarization origin.

From the observational point of view, the polarization as a function of photon energy for different fixed viewing angles is more convenient. Figure 3 depicts $\Pi(\varepsilon_1)$ for different viewing angles. In the top panel, $\Pi_0 = 0.75$. For $\theta = 0$, one can always observe a uniform 75% polarization for all photons. For $\theta = 0.005$, which corresponds to the first “valley” in the top panel of Figure 2, the polarization gradually goes to zero as the energy increases to 100 MeV. For $\theta = 0.01 \sim 2/\Gamma$, Π starts from 40% for $\varepsilon_1 < 1$ MeV and asymptotically goes to zero. For $\theta = 0.02$ and 0.05 , the polarization degree goes quickly to zero for photons with energy less than 10 MeV, and the polarization direction does not change. In the bottom panel, we set Π_0 to be zero. No scattering happens for $\theta = 0$, so no polarization will be observed. For $\theta = 0.005$, which corresponds to the maximal polarization induced by CS. Π goes to zero when ε_1 varies from 1 MeV to about 100 MeV.

A contour representation of the polarization is shown in Figure 4, the energy band is 10 keV – 1 GeV and $\Gamma\theta$ is in the range 0 – 4. The top panel depicts the SR induced initial polarization, and the bottom panel describes that the initial beam is unpolarized. Toma et al. (2009) calculated the polarization in the Compton drag model by using the stokes parameters, and showed that the maximal polarization degree occurs when $\theta \sim 1/\Gamma$. The similar results are also obtained by Lazzati et al. (2004). In Figure 4, we show that high level polarization occurs in both the initially polarized and unpolarized cases. In the top panel, the initial polarization can be observed for $\Gamma\theta \ll 1$, and there is no limit on the photon energy. The second large polarization occurs for $\Gamma\theta \sim 1$ and $\varepsilon_1 < 20$ MeV, very hard gamma-rays are unpolarized at this view angle. However, the probability to detect this regime is strongly suppressed by the small cross section. The third high polarized regime is $\Gamma\theta > 3$ and $\varepsilon_1 < 0.1$ MeV, the maximal polarization is roughly 75%, this is predicted by the CS process in the Thomson limit. The polarization is negligible at the region of $\Gamma\theta > 2$ and $\varepsilon_1 > 20$ MeV. The bottom panel in Figure 4 shows the polarization in the $\Pi_0 = 0$ case. One can also see the high polarized regime, where $\Gamma\theta \sim 1$ and $\varepsilon_1 < 20$ MeV. The grey area shows the forbidden parameter region.

The total intensity after scattering is $J' = J'_{\parallel} + J'_{\perp}$, where J'_{\parallel} and J'_{\perp} are given in Equations (4) and (5)¹. Under Lorentz transformation, the received intensity transforms as $J = \mathcal{D}^4 J'$ (Rybicki & Lightman 1979). The incident intensity I' transforms as $I' = \mathcal{D}_0^{-4} I_0$, where I_0 is the observed intensity at $\theta = 0$. Using Equation (2), we write the scattered intensity in the observer

¹Here we ignore a normalization factor, i.e., the total cross section σ_{total} .

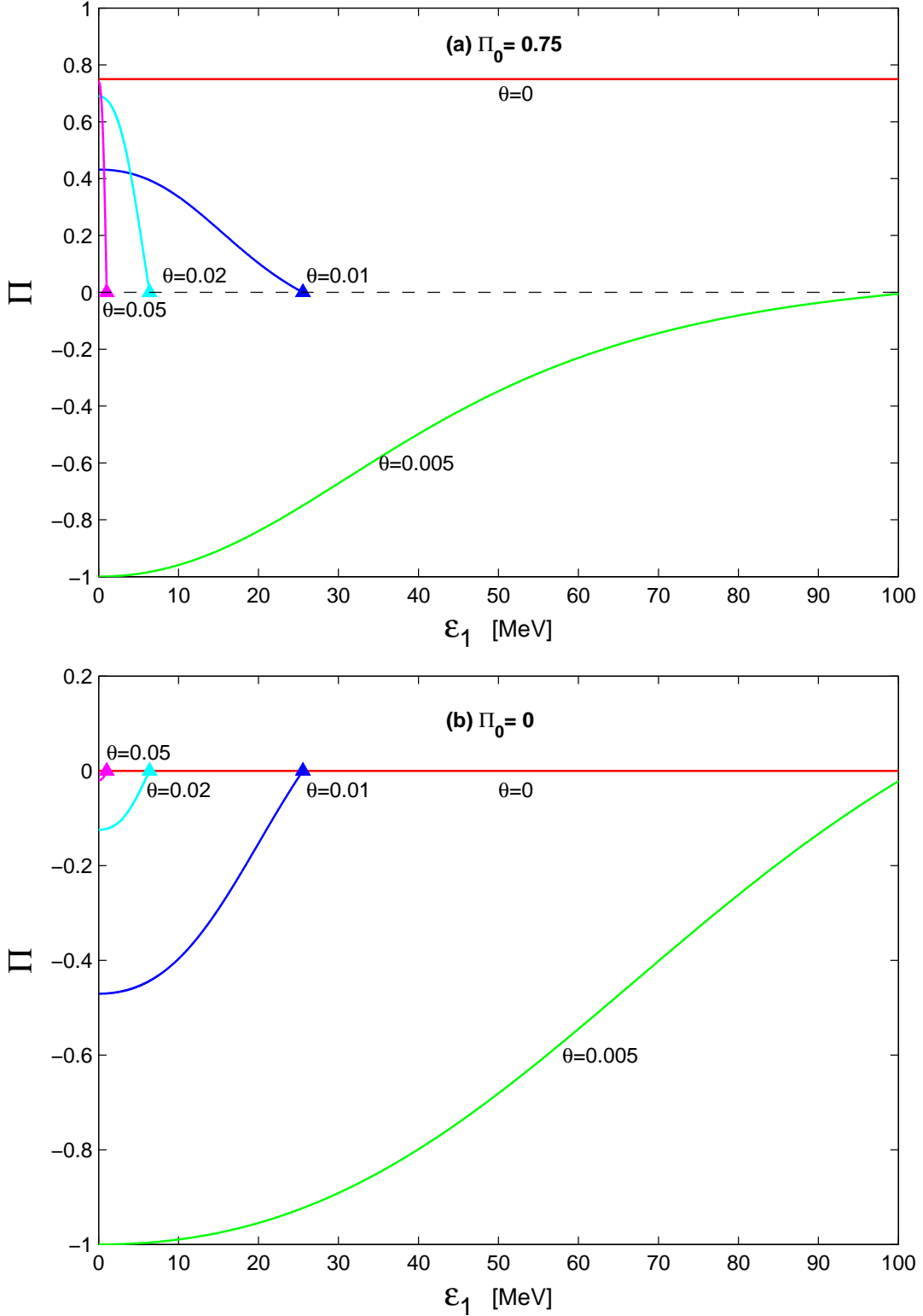


Fig. 3.— Polarization as a function of the observed photon energies. The initial polarization is set to be $\Pi_0 = 0.75$ in the top panel, and $\Pi_0 = 0$ in the bottom panel. Polarization curves for different viewing angles $\theta = 0, 0.005, 0.01, 0.02$ and 0.05 are plotted.

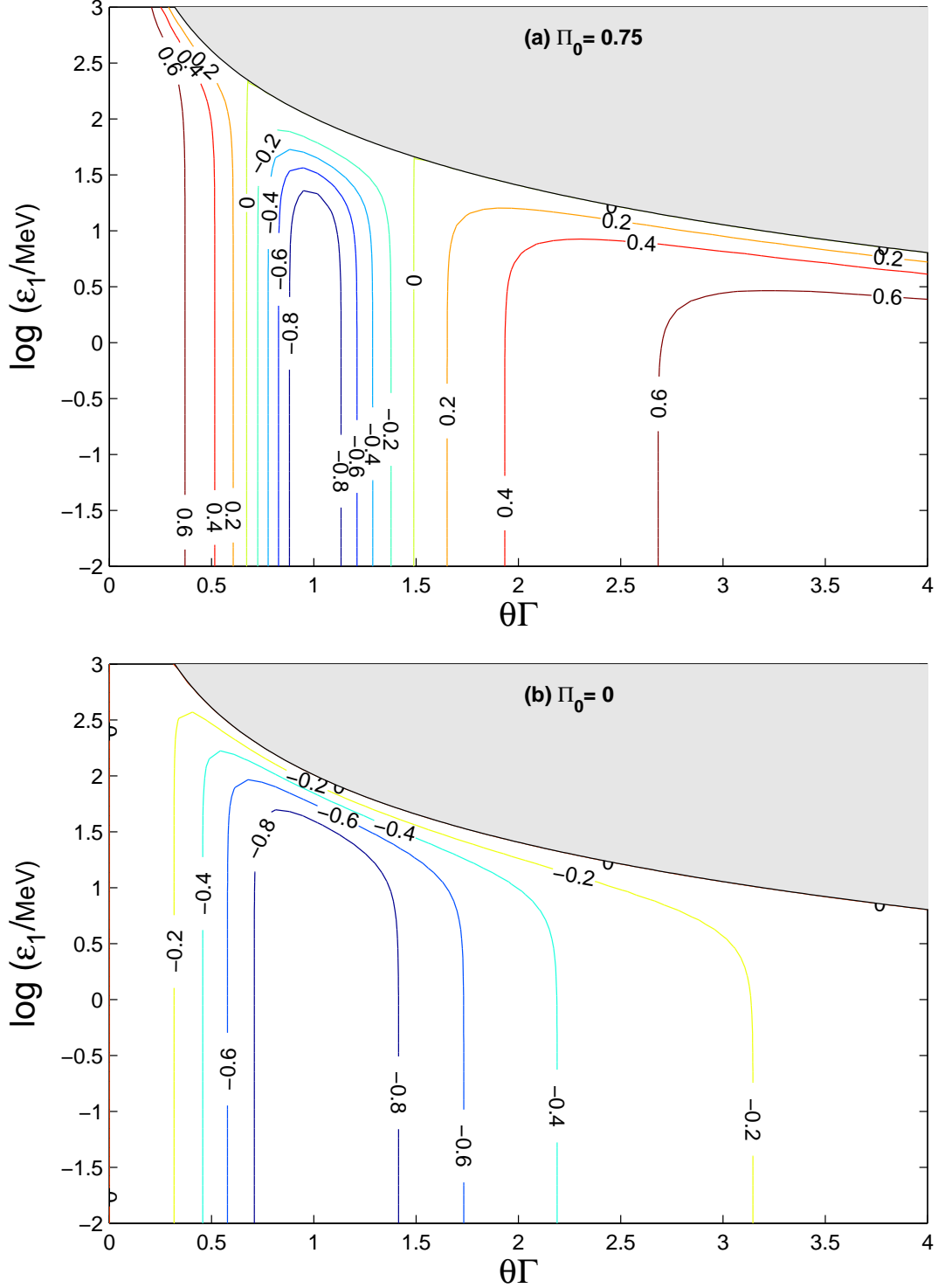


Fig. 4.— The contour representation of the polarization for $10 \text{ keV} < \varepsilon_1 < 1 \text{ GeV}$ and $0 < \Gamma\theta < 4$. We set $\Pi_0 = 0.75$ in the top panel and $\Pi_0 = 0$ in the bottom panel.

frame as

$$J = \frac{r_0^2}{2\sigma_{\text{total}}} I_0 \left(\frac{1 - \beta}{1 - \beta \cos \theta} \right)^4 \Sigma^2 \left[\Sigma + \Sigma^{-1} - (1 + \Pi_0) \frac{\sin^2 \theta}{\Gamma^2 (1 - \beta \cos \theta)^2} \right]. \quad (11)$$

In Figure 5, we used the contour representation to express the intensity as a function of the energy and scattering angle. The intensity decays rapidly to zero when $\Gamma\theta$ is asymptotic to 1, which means that the probability to detect the high polarization is strongly suppressed.

We mainly discuss the polarization induced by the CS process between gamma-rays and cold electrons. Such Compton processes do not change the original photon spectra significantly. The first reason is that the optical depth is less than one in this regime. The typical peak photon energy of the spectra is about 200 keV in the observer frame. It is 1 keV in the comoving frame if the bulk Lorentz factor of the jet is $\Gamma \sim 200$. Hence, photons in the prompt phase satisfy $\epsilon'_0 \gamma' / m_e c^2 \ll 1$ ($\gamma' = 1$ is the Lorentz factor of cold electrons in the comoving frame), and the CS is in the Thomson limit. Therefore, the photon energy is almost the same before and after scattering. For several hundred MeV photons, the head on collision will transfer the majority of the photon energy to the electron, so the CS processes will reduce the number of high energy photon events. This may be the reason for that the LAT (One instrument on the Fermi satellite which detects the energy range from 30 MeV to 300 GeV) photons are only observed in few GRBs. It has been argued that the Compton induced polarization requires a large energy budget (Coburn & Boggs 2003). If the scattered photons are isotropic in the comoving frame, the observed gamma-rays take only a fraction $d\Omega'/4\pi$ of the total emission. However, this is not the case in the system of the present paper due to the Lorentz effects. Although the angle distribution of scattered beam is nearly isotropic in the comoving frame, the scattered beam is emitted in a small cone in the observer frame.

One attractive feature of the Compton processes induced polarization is that the polarization can be as high as 100%. In the SR induced case, the polarization depends on both the configuration of the magnetic fields and the electron spectral index p . Considering a uniform magnetic field at large scale with the most ideal configuration, $\Pi_{\text{max}} = (p + 1)/(p + 7/3) < 80\%$ for $p < 4$. The shock accelerated electrons have a typical spectral index $p = 2.3$, this predicts $\Pi_{\text{max}} = 71\%$. Therefore, the CS process is the most probable to account for the observation of $\Pi > 80\%$. One can not exclude the SR as the major emission mechanism in the prompt phase by observing $\Pi > 80\%$, since $\Pi = 100\%$ at $\Gamma\theta = 1$ occurs in both the $\Pi_0 = 0$ and the $\Pi_0 = 0.75$ cases. Also at this right viewing angle, the polarization direction changes 90° relative to the incident polarization direction.

The analysis of the intensity also indicates that the scattered beam is relatively dimmer at $\Gamma\theta = 1$. This means that the chance to detect the high polarization is small. However, this difficulty can be overcome with certain specific configurations. Levinson & Eichler (2004) considered the polarization caused by gamma-rays scattered off the coasting baryon walls by the Compton sailing. There is a thick baryon wall in the out layer of the jet, and the inner core of the jet is baryon poor. This leads to the coincidence of the angle of the maximal polarization and the angle of the maximal intensity. If we consider the similar wall sheath configuration, but replace the baryon materials with the cold electrons, the viewing angle coincidence of the maximal intensity and the maximal

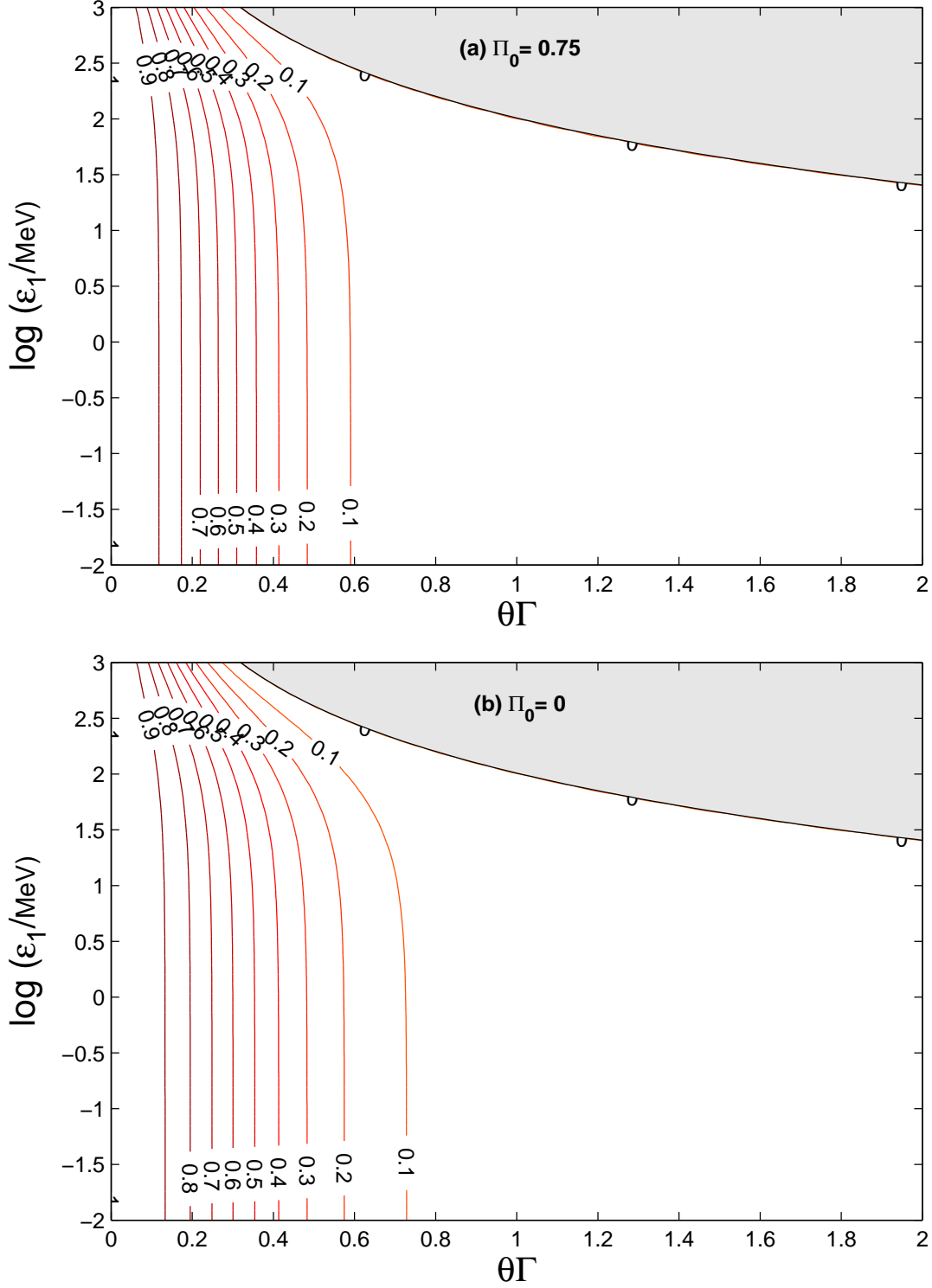


Fig. 5.— The contour representation of the intensity in unit of $r_0^2 I_0 / \sigma_{\text{total}}$. We set $\Pi_0 = 0.75$ in the top panel and $\Pi_0 = 0$ in the bottom panel.

polarization can be realized. Our derivation of the polarization is based on the point source, it still holds when the emission regime of the jet is a small surface. In the narrow jet scenario with $\Gamma\theta_{\text{jet}} < 1$, our results in Equation (10) roughly holds. When the emission surface is large, i.e. $\Gamma\theta_{\text{jet}} > 1$, the maximal polarization becomes small (Lazzati et al. 2004).

The polarization of SR photons is independent of the energy, but the CS induced polarization does depend on the energy. If Γ is larger, for instance $\Gamma = 1000$, 2 MeV photons have smaller polarization than 1 MeV photons. The broad energy band detection of polarization is necessary to verify the CS induced polarization. This gives us a trend that higher energy photons have smaller polarization, which distinguishes from that of the SR induced polarization.

An observer collects radiations from different emission regions with different viewing angles. The averaged polarization should consider such net polarization effect. The geometry of the scattering region is assumed to be a plane, and the integral range depends on the size of the plane. Other structures of the jet are also possible, which can be studied case by case. For simplicity, we set $\varepsilon_1 = 0.1$ MeV, which is the typical value of the observed gamma-rays. Both the polarization and the intensity are only functions of $\Gamma\theta$. The averaged polarization can be written as

$$\langle \Pi \rangle = \frac{\int_{x_1}^{x_2} \Pi(x)J(x)dx}{\int_{x_1}^{x_2} J(x)dx}, \quad (12)$$

where $x \equiv \Gamma\theta$ and the integration range is from x_1 to x_2 . Since the intensity J is almost zero when $x \sim 1$, we take $x_1 = 0$ and $x_2 = 1$. For $\Pi_0 = 0.75$, we obtain $\langle \Pi \rangle \approx 65\%$. Hence, the CS process reduces the initial polarization. For $\Pi_0 = 0$, we obtain $\langle \Pi \rangle \approx 20\%$. For randomly oriented magnetic fields with N patches, the initial SR induced polarization degree is $\Pi_0 = \Pi_{\text{max}}/\sqrt{N}$, which can change $\langle \Pi \rangle$ significantly. If the jet opening angle is small, i.e. $\theta_{\text{jet}} \ll \Gamma^{-1}$, the integral range becomes small. In this way, the averaged polarization is mainly determined by the specific viewing angle. The probability of the CS process is relative to the optical depth $\tau = \sigma_T nR$, where the number density of cold electrons n is an unknown parameter. If $\tau < 1$, one should also consider the mixing effect of the scattered and un-scattered photons. Considering all these ingredients, the SR plus CS model predicts a wide range of the polarization.

3. Against GRBs cases

We mainly concentrate on the polarization analysis in the prompt emission. Coburn & Boggs (2003) reported a very large linear polarization $\Pi = 80\% \pm 20\%$ in the prompt phase of GRB 021206 observed by *RHESSI*. However, other independent groups did not confirm the polarization signals using the same data (Rutledge & Fox 2004; Wigger et al. 2004). Similar debates also occurred in GRB 041219A (Kalemci et al. 2007; McGlynn et al. 2007; Götz et al. 2009). The instrumental systematics are the main obstacle to get a convincing result (Yonetoku et al. 2011). In the following, we will discuss polarizations in GRB 041219A (McGlynn et al. 2007), GRB 100826A (Yonetoku et al. 2011), GRB 110301A and GRB 110721A (Yonetoku et al. 2012).

GRB 041219A is an intense burst detected by the *INTEGRAL*. The polarization measurement in the brightest 12 s interval and the total 66 s interval was performed in the energy ranges 100–300 keV, 100 – 500 keV and 100 keV–1 MeV, respectively. With the 6 scattered directions analyses, the polarization of the 12 s interval is $98^{+2}_{-53}\%$ in the range 100 – 350 keV and $71^{+29}_{-53}\%$ in the range 100 – 500 keV (McGlynn et al. 2007). Furthermore, the 3 directions analyses of the 12 s interval shows the polarization to be $96^{+39}_{-40}\%$, $70 \pm 37\%$ and $68 \pm 29\%$ in the three respective energy ranges. The Compton processes predict that the polarization of high energy photons is smaller than that of $E < 1$ MeV photons at $\Gamma\theta \sim 1$, and the critical energy is 10 MeV. In order to lower the critical energy to 1 MeV, one needs Γ up to 2000. The high luminosity of the burst means that the viewing angle is not likely to be $\theta \sim \Gamma^{-1}$, unless the geometry structure of the jet is similar to the baryon-wall structure given in Levinson & Eichler (2004). Beyond the two conditions, the high polarization is most probably caused by the SR. Since the system uncertainty is large, a confirmative conclusion is difficult to give.

Yonetoku et al. (2011) reported the polarization of GRB 100826A measured by *IKAROS*. The average polarization is $27\% \pm 11\%$ in the energy range 70 – 300 keV with 2.9σ confidence level. A change of polarization angle during the prompt phase was confirmed with 3.5σ confidence level. GRB 100826A is the top 1% of the brightest events listed in the *BATSE* catalog. The peak energy is $E_p = 606^{+134}_{-109}$ keV, and the low and high energy band indices are $\alpha = -1.31^{+0.06}_{-0.05}$ and $\beta = -2.1^{+0.1}_{-0.2}$, respectively. This spectrum can be explained by the synchrotron radiation both in the fast and the slow cooling phases. The data of the two intervals, each with the duration of 50 s, give $\Pi_1 = 25\% \pm 15\%$ with $\phi_1 = 159 \pm 18$ deg for Interval 1 and $\Pi_2 = 31 \pm 21\%$ with $\phi_2 = 75 \pm 20$ deg for Interval 2, respectively. The pulse in Interval 1 is more intense than that in Interval 2. With the SO model, Yonetoku et al. (2012) argued that the polarization angle change in GRB 110826A is due to many patches of the magnetic fields. The angle size of the magnetic fields satisfies $\theta_p \ll \theta_{\text{jet}}$, where θ_{jet} is the jet opening angle. One can only observe an angle size of Γ^{-1} along the line of sight. If $\theta_{\text{jet}} \sim \Gamma^{-1}$, many pathes can be observed, and the polarization angle change is possible. However, this can not explain why the polarization angle change is 90° exactly.

If the initial jet opening angle is small, the polarization angle changing can be explained by the changing of the viewing angle in the SR plus CS model. During the first interval, the line of sight moves away from near the axis of the jet. In the range $1/2 < \Gamma\theta < 2/3$ ($\Pi = 0$ when $\Gamma\theta \approx 2/3$), the SR induced polarization is dominated, and the average polarization is estimated to be 28% according to Equation (12). This value is positive, referring the top panel in Figure 2. In the range $2/3 < \Gamma\theta < 1$, the averaged polarization is 40% with a minus sign, i.e., the polarization angle changes 90° . Also the intensity in the second viewing angle range is smaller than the intensity in the first one. Then beyond $\Gamma\theta > 1$, the intensity almost disappears. And correspondingly, no respective pules is reported in observation. One can also infer that $\theta_{\text{jet}} \sim \Gamma^{-1}$ in this burst. Therefore, the averaged polarization, the polarization angle and the light curves of the GRB 100826A can be well described in the SR plus CS model .

Finally, we discuss the recent polarization measurements in GRB 110301A and GRB 110721A

(Yonetoku et al. 2012). Compared with GRB 100826A, no polarization angle change was detected in these two bursts, the polarization is $\Pi = 70\% \pm 22\%$ (3.7σ) for GRB 110301A and $\Pi = 84^{+16}_{-28}\%$ (3.3σ) for GRB 110721A. Yonetoku et al. (2012) explained that the synchrotron model can be consistent with these two GRBs, the magnetic field structures are globally ordered and advected from the central engine. GRB 110301A has a short time duration, $T_{90} = 5$ s, and the peak energy is about $E_{\text{peak}} = 106.80$ keV (Foley et al. 2011). The Band spectra gives $\alpha = -0.81$ and $\beta = -2.70$. One can obtain the index of electrons via the relation $\beta = -(p + 1)/2$, i.e. $p = 4.4$. The SO model predicts $\Pi = 80\%$, consistent with the observation. GRB 110721A has an unusual high energy peak $E_{\text{peak}} \sim 15$ MeV (Axelsson et al. 2012), the dissipative photosphere synchrotron model can account for such high peak values whether the outflow is extreme magnetic-dominated or baryon-dominated (Veres et al. 2012). The gamma-ray burst polarimeter aboard the *IKAROS* mainly observes the energy range 70 – 300 keV, which coincides with the blackbody component with temperature ranging in 10 – 100 keV. However, the flux of the blackbody component is small compared to the non-thermal component, and the polarization reduction is less important. The low energy index of the Band spectra is $\alpha \approx -1$, which is the mostly observed value in GRBs. The SR in the fast cooling phase predicts $\alpha \sim -2/3$. Some authors suggested that the IC scattering in the Klein-Nishina regime plays an important role to tune α to approach the -1 limit (Nakar et al. 2009; Duran et al. 2012). The IC processes in the hot plasma will reduce the polarization to a neglectful level. Meanwhile, the energies of the scattered photons are also shifted to the high energy range $E > 1$ MeV. The observed photons in the energy range 70 – 300 keV are due to the low energy tail of the SR. The observed high polarization can not exclude the self-synchrotron Compton (SSC) origin.

4. Conclusions and remarks

We showed that the synchrotron photons collide with cold electrons in the jet can significantly change both the polarization degree and the polarization direction. The photons are not up-scattered, but transfer energies to electrons. Due to the Klein-Nishina effects, high energy photons ($E > 10$ MeV) have smaller polarization than low energy photons ($E < 1$ MeV). After scattering, the polarization angle changes 90° relative to the original direction, and the polarization reaches the maximal value at the right viewing angle $\Gamma\theta \sim 1$. These results indicate that the high polarization may also caused by the CS process. The jet structure is essential for the net polarization, we leave this topic for future study.

The polarimetry of the prompt emission can be used to distinguish the GRB models. In the SO model, the prompt emission is due to the synchrotron radiation, an ordered magnetic fields can produce large polarization. The SO model predicts that the polarization is universal for photons with different energies, the unknown geometry of the emitting region also affects the observed results (Granot 2003; Nakar et al. 2003). Recently, the deviations from the Band function in the low energy range have been discussed by Tierney et al. (2013). For instance, a Band plus blackbody fit

is better than a single Band fit in the GRB 090323. The thermal component occurs naturally in the photosphere internal shock model (Toma et al. 2011). The thermal photons have no polarization initially. After up-scattered by the electrons with power-law distribution via IC processes, the observed photons are linearly polarized. The linear polarization degree is anticorrelated with the weight of the thermal component. Therefore, the polarization in the low energy range is less than that in the high energy range. This prediction is quite different with the prediction in our SR plus CS scenario. The high polarization can be obtained from the edge of a narrow jet, although the probability is not high (Fan 2009)². Zhang & Yan (2011) proposed the internal-collision-induced magnetic reconnection and turbulence (ICMART) model to explain GRB 080916C. The internal shock distorts the ordered magnetic fields, and further the magnetic turbulence triggers the prompt emission. One ICMART event corresponds to one pulse in the GRB light curve. The linear polarization degree evolves during one pulse. In the beginning of one pulse, the polarization degree achieves the maximal value of SR, i.e., $\Pi \sim 50\% - 70\%$. At the end of the pulse, the ordered magnetic field structure is destroyed, and the reasonable net polarization is less than 10%. The average value of the polarization in one pulse is estimated to be around 30%, close to that observed in GRB 100826A. However, a physical scenario to explain the 90° angle changing in the two intervals is still missing. In summary, the polarization can help us a lot to understand the prompt emission.

We thank the anonymous referee for very helpful suggestions and comments. We are grateful to Li M. H., Li X. and Wang S. for useful discussion. This work has been supported in part by the NSF of China under Grant No. 11075166 and No. 11147176. Jiang Y. is also funded by the China Postdoctoral Science Foundation funded project Grant No. 2012M510548.

REFERENCES

- Amarti, L., et al. 2002, *A&A*, 390, 81
Amarti, L. 2006, *MNRAS*, 372, 233
Axelsson, M., et al. 2012, *ApJ*, 757, L31
Band, D., et al. 1993, *ApJ*, 413, 281
Berger, E., et al. 2011, *GCN Circ.* 12193
Bersier, D., et al. 2003, *ApJ*, 583, L63

² Our SR plus CS scenario is similar to Fan’s set-up except two differences. One difference is that the incident photons are polarized in our scenario and not polarized in Fan’s scenario. The other difference is that we considered cold electrons, while Fan considered the electrons with isotropic distribution. We leave the study the polarization induced by the polarized incident photons and isotropic electrons to be the near future work.

- Caldwell, N., Garnavich, P., Holland S., Matheson, T., & Stanek, K. Z. 2003, GCN Circ. 2053
- Chang, Z., Jiang, Y., & Lin H. N. 2012, *Astroparticle Physics*, 36, 47
- Chang, Z., Lin, H. N., & Jiang, Y. 2012, *ApJ*, 759, 129
- Coburn, W., & Boggs, S. E. 2003, *Nature*, 423, 415.
- Cocke, W. J., & Holm, A. A. 1972, *Nature Physical Science*, 240, 161
- Covino, S., et al. 1999, *A&A*, 348, L1
- Covino, S., et al. 2003, *A&A*, 400, L9
- Daigne, F., Bošnjak, Ž., & Dubus, G. 2011, *A&A*, 526, 110
- Duran, R. B., Bošnjak Ž., & Kumar, P. 2012, *MNRAS*, 424, 3192
- Eichler, D., & Levinson, A. 2003, *ApJ*, 596, L147
- Fan, Y. Z., 2009, *MNRAS*, 397, 1539
- Foley, S., et al. 2011, GCN Circ. 11771
- Frail, D. A., Kulkarni, S. R., Bloom, J. S., & Djorgovski, S. G. 1998, GCN Circ. 147
- Götz, D., et al. 2009, *ApJ*, 695, L208
- Granot, J. 2003, *ApJ*, 596, L17
- Greiner, J., et al. 2003, *Nature*, 426, 157
- Gruzinov, A., & Waxman, E. 1999, *ApJ*, 511, 852
- Gruzinov, A. 1999, *ApJ*, 525, L29
- Hjorth, J., et al. 1999, *Science*, 283, 2073
- Kalemci, E., Boggs, S. E., Kouveliotou, C., Finger, M., & Baring, M. G. 2007, *ApJS*, 169, 75
- Lazzati, D., et al. 2003, *A&A*, 410, 823
- Lazzati, D., Rossi, E., Ghisellini, G., & Rees, M. J. 2004, *MNRAS*, 347, L1
- Levinson, A., & Eichler, D. 2004, *ApJ*, 613, 1079
- Lyutikov, M., Pariev, V. I., & Blandford, R. D. 2003, *ApJ*, 597:998
- McGlynn, S., et al. 2007, *A&A*, 466, 895
- Nakar, E., Piran, T., & Waxman, E. 2003, *JCAP*, 10, 5

- Nakar, E., Ando, S., & Sari, R. 2009, *ApJ*, 703, 675
- Preece, R. D., et al. 2000, *ApJS*, 126, 19
- Rossi, E. M., Lazzati, D., Salmonson, J. D., & Ghisellini, G. 2004, *MNRAS*, 354, 86
- Rutledge, R. E., & Fox, D. B. 2004, *MNRAS*, 350, 1288
- Rybicki, G. B., & Lightman, A. P. 1979, *Radiative Processes in Astrophysics* (New York: Wiley)
- Sari, R., Piran, T., & Narayan, R. 1998, *ApJ*, 497, L17
- Sari, R. 1999, *ApJ*, 524, L43
- Shaviv, N. J., & Dar, A. 1995, *ApJ*, 447, 863
- Steele, I. A., Mundell, C. G., Smith, R. J., Kobayashi, S., & Guidorzi, C. 2009, *Nature*, 462, 767
- Taylor, G. B., et al. 1998, *ApJ*, 502, L115
- Tierney, D., et al. 2013, *A&A*, 550, A102
- Toma, K., et al. 2009, *ApJ*, 698, 1042
- Toma, K., Wu, X. F., & Mészáros, P. 2011, *MNRAS*, 415, 1663
- Toma, K., et al. 2012, *Phys. Rev. Lett.*, 109, 241104
- Uehara, T., et al. 2012, *ApJ*, 752, L6
- Veres, P., Zhang, B. B., & Mészáros, P. 2012, *ApJ*, 761, L18
- Wiersema, K., et al. 2012, *MNRAS*, 426, 2
- Wigger, C., Hajdas, W., Arzner, K., Güdel, M., & Zehnder, A. 2004, *ApJ*, 613, 1088
- Wijers, R. A. M. J., et al. 1999, *ApJ*, 523, L33
- Yonetoku, D., et al. 2011, *ApJ*, 743, L30
- Yonetoku, D., et al. 2012, *ApJ*, 758, L1
- Zhang, B., & Yan, H. R., 2011, *ApJ*, 726, 90